Ultra-flexible Corrugated Monocrystalline Silicon Solar Cells with High Efficiency (19%), Improved Thermal Performance and Reliability Using Low-Cost Laser-Patterning

Nazek El-Atab[§], Wedyan Babatain[§], Rabab Bahabry[‡], Reem Alshanbari[§], Rana Shamsuddin[†], Muhammad Mustafa Hussain[§,⊥]*

[§]MMH Labs, Electrical Engineering, Computer Electrical Mathematical Science and Engineering Division, King Abdullah University of Science and Technology (KAUST), Thuwal 23955-6900, Saudi Arabia

[‡]Department of Physics, University of Jeddah, Jeddah 21589-80200, Saudi Arabia

[†]Department of Physics, King Abdulaziz University (KAU), Jeddah 21589-80200, Saudi Arabia

[⊥]EECS, University of California, Berkeley, California, USA

Corresponding Author

Email addresses: muhammad.hussain@kaust.edu.sa and mmhussain@berkeley.edu

ABSTRACT. Flexible solar cells have received a growing attention recently due to their ever-increasing range of applications. Here, the development of ultra-flexible, lightweight and high-efficiency (19%) monocrystalline silicon solar cells with excellent reliability, mechanical resilience and thermal performance is demonstrated by applying a corrugation method combined with laser-patterning. The flexing mechanism converts large-scale rigid photovoltaic cells with interdigitated back contacts into a flexible version with a preserved efficiency. The corrugation technique is based on the formation of patterned grooves in the active silicon to achieve ultra-flexibility. As a result, islands of silicon with different shapes are obtained which are interconnected through the IBC. Multiple corrugation patterns are studied such as linear, honeycomb and octagonal designs, each resulting in different flexing capability in terms of flexing directionality and minimum bending radius, in addition to providing an atypical appearance with an aesthetic appeal. The corrugation method is shown to improve the thermal dissipation (14.6% lower temperature) and to relieve the thermal mismatch challenge compared to the rigid cells due to the fin-like architecture. Finally, the encapsulation using a transparent polymeric material enables a robust performance of the flexible cells when exposed to different environmental conditions such as acid rain, snow and mechanical shocks.

KEYWORDS. Solar cells, monocrystalline silicon, interdigitated back contacts, flexible, corrugation, thermal performance, encapsulation.

INTRODUCTION

The development of high efficiency and flexible solar cells is driven by the rapid market growth of a wide range of applications including, but not limited to, robotics, wearables, and curved skyscapers in highly packed cities.[1-6] The main advantages of flexible solar cells lie in their ability to conform to curved surfaces, their lightweight and portability. Even though different materials are being continuously studied and enhanced for the development of flexible solar cells such as III-V semiconductors and organic materials,[7-13] however, silicon remains the material of choice in photovoltaic inductry due to its optimum bandgap for sunlight absorption resulting in a good efficiency, excellent reliability, low toxicity, abundant raw material supply, low cost and maturity of the manufacturing process.[14-19]

In the last years, several high efficiency (> 25%) rigid silicon solar cells have been reported, mainly driven by the interdigitated back contact (IBC) structure and passivated contacts.[20-24] As a matter of fact, the back contact architechtures achieve substantial enhancement in short circuit current as a result of zero shading losses, simpler interconnection schemes with improved packing density, better aesthetics, reduced resistive losses and therefore higher efficiencies.[26] Moreover, since front surface doping is no longer required in IBC structures, the optical performance of the solar cell can be optimized using a wider range of front surface light trapping schemes and texturing. [27-29] As a result, the IBC strcuture has long been believed to be paving the way to the theoretical limit of silicon solar cells' efficiency. Therefore, developing new

techniques to transfrom large-scale commerical silion solar cells based on the IBC technology into an ultra-flexible version with a preserved efficiency would be crucial for the development of flexible silicon photovoltaics with the largest possible efficiency.

Previously, we have demonstrated a lithography-less corrugation technique that transforms large-area rigid solar cells based on the IBC technology into flexible and stretchable ones with no deterioration in the original efficiency.[30-31] A world record minimum bending radius (140-μm) was shown, however, with an area loss of~15% of the active silicon.[30] Moreover, due to the linear corrugation, flexing in one direction was only possible.[30] Here, different corrugation patterns (diamond, honeycomb, hexagonal and octagonal) are studied using laser patterning to achieve ultra-flexibility with minimal losses in the active silicon area (down to 5.6%). The presented results provide a guideline for meeting the requirements of a specific solar cells' application in terms of flexibility, weight and output power. The effect of the corrugation structure on the thermal performance in terms of thermal dissipation and thermal mismatch stress is examined. Finally, the effect of a polymeric encapsulation on the electrical performance of the corrugated solar cells is studied after their exposure to different environmental settings.

1. RESULTS AND DISCUSSION

2.1. Fabrication and Flexing Directionality of the Patterned Solar Cells

To develop the flexible photovoltaic cells, a corrugation process is applied on commercially available large-scale monocrystalline silicon solar cells (5 inch by 5 inch) with interdigitated back contacts (IBC) and high efficiency (19%). The corrugation technique is based on a combination between CO_2 laser patterning and deep reactive ion etching (DRIE) (Figure 1a) to generate 138 μm-wide and 170 μm-deep grooves with different patterns, resulting in ultra-

flexible structures with different flexing capabilities and appealing designs (Figures 1b, 2). Polydimethylsiloxane (PDMS) polymeric material with a thickness of 160 μm is then used as the encapsulation material to improve the reliability and mechanical resilience of the solar cells (Figure 1b). As a result, the grooves are filled with PDMS, in addition, the backside of the cell is coated with PDMS. For all the designs, the distance between any two consecutive and parallel grooves is fixed at 4 mm (Figure 2a). It is worth to mention that a world record 1-directional stretchability in solar cells has been recently achieved by our group[31] by applying the corrugation technique on the commercial monocrystalline silicon solar cell with no deterioration in their original performance. However, an ultra-stretchable elastomer (Ecoflex) was coated on the cell's back side as a substrate instead of PDMS, in addition, specially engineered patterns were used (e.g. linear and triangular patterns separated by 1-mm gaps). In fact, stretchability requires that the micro-cells be aligned orthogonally to the applied tensile stress while this is not necessary for achieving flexibility as shown in the patterns depicted in Figure 1b.

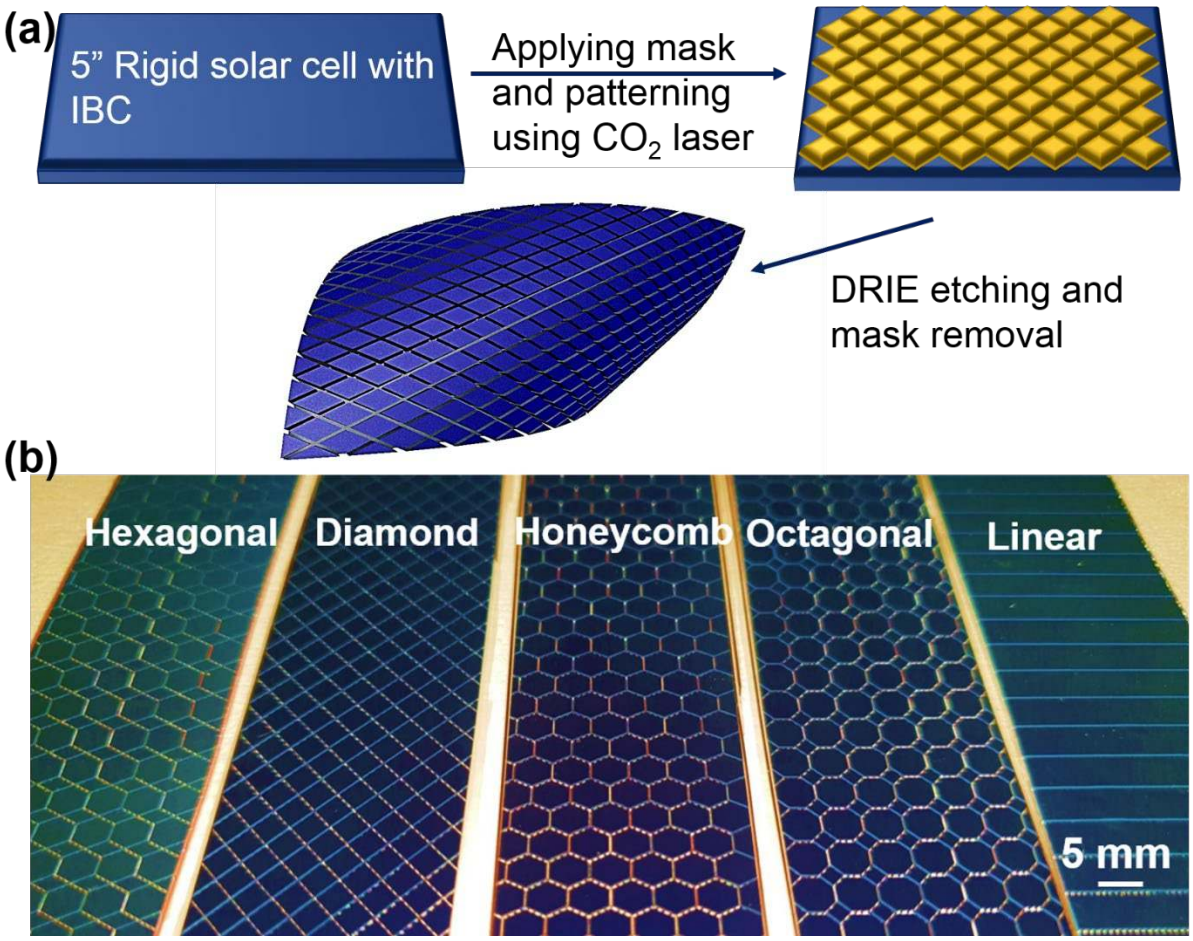

Figure 1. (a) Process flow of the flexible photovoltaic cells fabrication. The fabrication is conducted using a corrugation technique where alternate grooves are created in commercially available monocrystalline solar cells. (b) Optical image shown the five corrugation patterns that are studied including: hexagonal, diamond, honeycomb, octagonal and linear structures.

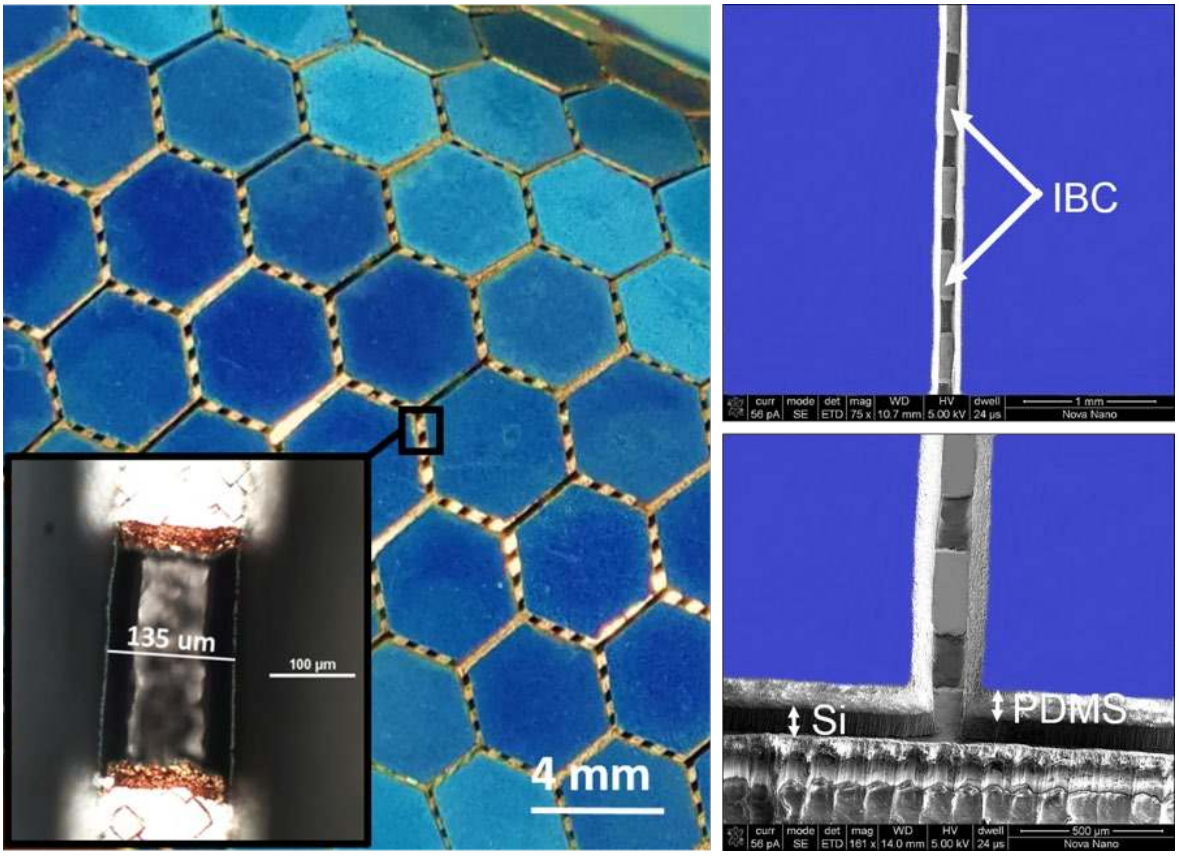

Figure 2. Optical and scanning electron microscopy images of the hexagonal corrugated solar cells showing the interdigitated back contacts structure. Inset shows the created grooves which are ~135-µm wide. The PDMS encapsulation is also shown on top of the silicon islands in the SEM cross-section figure.

The linear corrugated solar cells enable the flexing of the cells in one direction with a minimum bending radius of 5 mm. It is worth to note that wider grooves result in a smaller minimum bending radius.[28] On the other hand, the diamond, honeycomb, hexagonal and octagonal patterns allow the flexing of the cells in four specific directions with different capabilities. For instance, the diamond patterned cells can be flexed in a spiral way while hexagonal patterned cells show a dual curvature (Figures 3a-b). Moreover, even though the

studied patterns allow the bending of the cells in four directions, the minimum bending radius for each direction is different and is limited by the area and depth of the rigid overlapping silicon area along the bending axis. For instance, regarding the diamond patterned cell, when the cells are flexed along the x/y directions, no rigid overlapping area exists resulting in a 5 mm minimum bending radius (similarly to the linearly patterned cells case). While when the diamond patterned solar cells are flexed along the v/w directions, the rigid overlapping silicon area limits the minimum bending radius to 1.5 cm. The same applies to the honeycomb, hexagonal and octagonal patterns where a larger rigid overlapping area with a larger depth increase the minimum bending radius. In summary, the width of the grooves determines the minimum bending radius in the case of corrugation patterns where no rigid area is overlapping along the bending axis such as the case of linear and diamond patterned cells (along x/y directions). While in the case of corrugation patterns where a rigid overlapping area exists along the bending axis, the two main characteristics that dictate the minimum bending radius are the overlapping area and its depth, unlike the case of corrugation-based stretchable solar cells where the orthogonality of the rigid islands to the applied tensile stress determines the maximum achievable stretchability. The minimum bending radii are then extracted under an optical microscope, beyond which the silicon islands start to peel off of the IBC (Figures 3c-d). Table 1 notes the measured minimum bending radii of all the studied corrugation patterns along the different axes (Figures 3e-f).

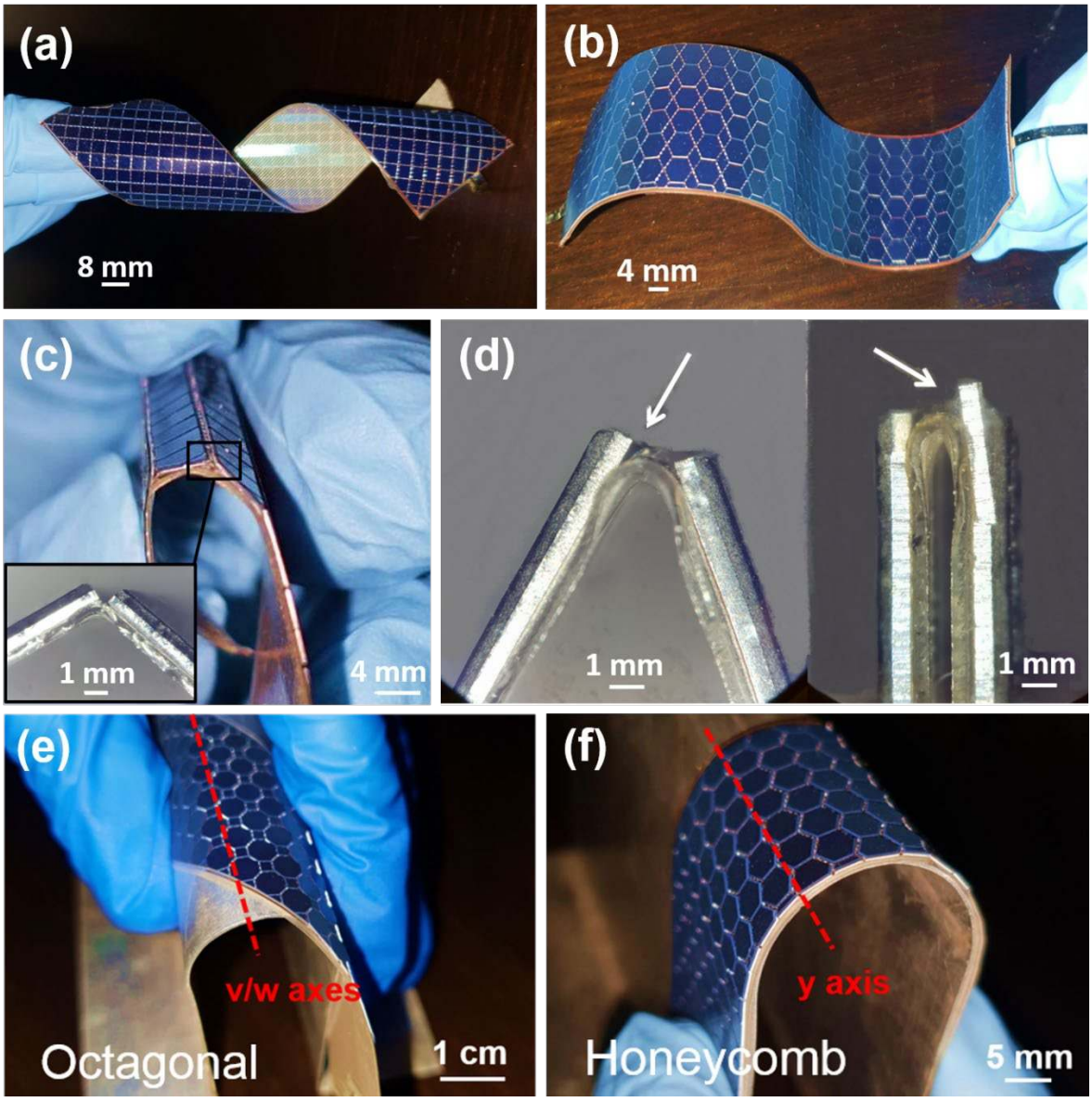

Figure 3. (a) Optical image of the diamond corrugated photovoltaic cell flexed in a spiral way. (b) Optical image of the hexagonal corrugated photovoltaic cell showing flexing capability with dual curvature. (c) Optical image of the diamond corrugated photovoltaic cell flexed along its y-axis. Inset showing the minimum bending radius of the structure before the silicon starts to peel off of the substrate. (d) Optical image showing the peeling off effect of the silicon from the IBC/PDMS substrate. (e) Optical image of the octagonal corrugated

photovoltaic cell bent along the v/w axis. (f) Optical image of the honeycomb corrugated photovoltaic cell bent along the y-axis.

Table 1. Flexing directionality and minimum bending radius of the different corrugated solar cells

Pattern	Directional Axis			
	x	y	m/n	v/w
Linear	5 mm	-	-	-
Diamond	5 mm	5 mm	-	1.5 cm
Honeycomb	6 mm	2 cm	6 mm	-
Hexagonal	6 mm	2 cm	-	1.1 cm
Octagonal	7.5 cm	7.5 cm	-	1.5 cm

2.2. Electrical Performance of the Flexible Solar Cells

The current density-voltage (J-V) and power density-voltage (P-V) characteristics of the rigid and flexible solar cells, with the same ground area (12.5×2.5 cm^2), are measured using a solar simulator in air (AM 1.5 Global Spectrum with 1000 Wm^{-2} intensity and spectral mismatch correction at ambient conditions). The J-V and P-V, standardized to the actual silicon area, show the capability of the corrugation process to convert rigid solar cells into their flexible version with insignificant deterioration in the electrical performance (Figures 4a-b). The average of the measured figures of merit are the following: short-circuit current $J_{sc} = 38.85 \pm 1.2$ cm^2, open-circuit voltage $V_{oc} = 0.64 \pm 0.05$ V, efficiency $\eta = 18.89 \pm 0.53\%$ and fill factor FF = 75.92 ± 0.7 %, where the error is the standard deviation from 10 characterized devices. In fact, the DRIE process is optimized (see Materials and Methods section) to result in low damage on the sidewalls. In addition, the exposed sidewalls, which are passivated using a fluorocarbon-based polymer,[32] increase photons absorption.[33] Finally, the created grooves increase the surface area-to-volume ratio of the solar cell and therefore improve thermal dissipation by natural convection.[34] These effects counteract any DRIE-induced damage effect.

It is worth to mention that the normalized area of the flexible solar cells takes into consideration the losses of the active silicon areas in the created grooves with different shapes. The actual loss of silicon area in the case of the different corrugation patterns is measured and calculated using an image processing software (Figures S1, S2, S3, S4). The linear corrugated solar cells show the smallest loss of active area (5.6%) while the octagonal patterns show the largest loss (18%) as shown in Figure 4c. The specific weights of the corresponding solar cells are measured and calculated (Figure 4c) where a larger loss of active silicon results in a lower specific weight. Thus, there is a tradeoff relationship between the specific weight and actual output power as shown in Figure 4d, where the power density is normalized to the ground area (12.5×2.5 cm^2) and not to the actual area of the active silicon. Therefore, for applications where the weight is a critical factor, flexible solar cells with a larger loss of active silicon would be used resulting in a lower power output. Moreover, it is important to note that the minimum bending radius of the flexible solar cells does not depend on the value of the loss of active area; instead, it depends on the corrugation pattern where the diamond patterned solar cell, for instance, shows a small loss of area (6.5%) with the smallest minimum bending radius along the x/y directions (5 mm). Thus, the corrugation patterns can be customized to meet the requirements of the application in terms of flexibility, weight and output power.

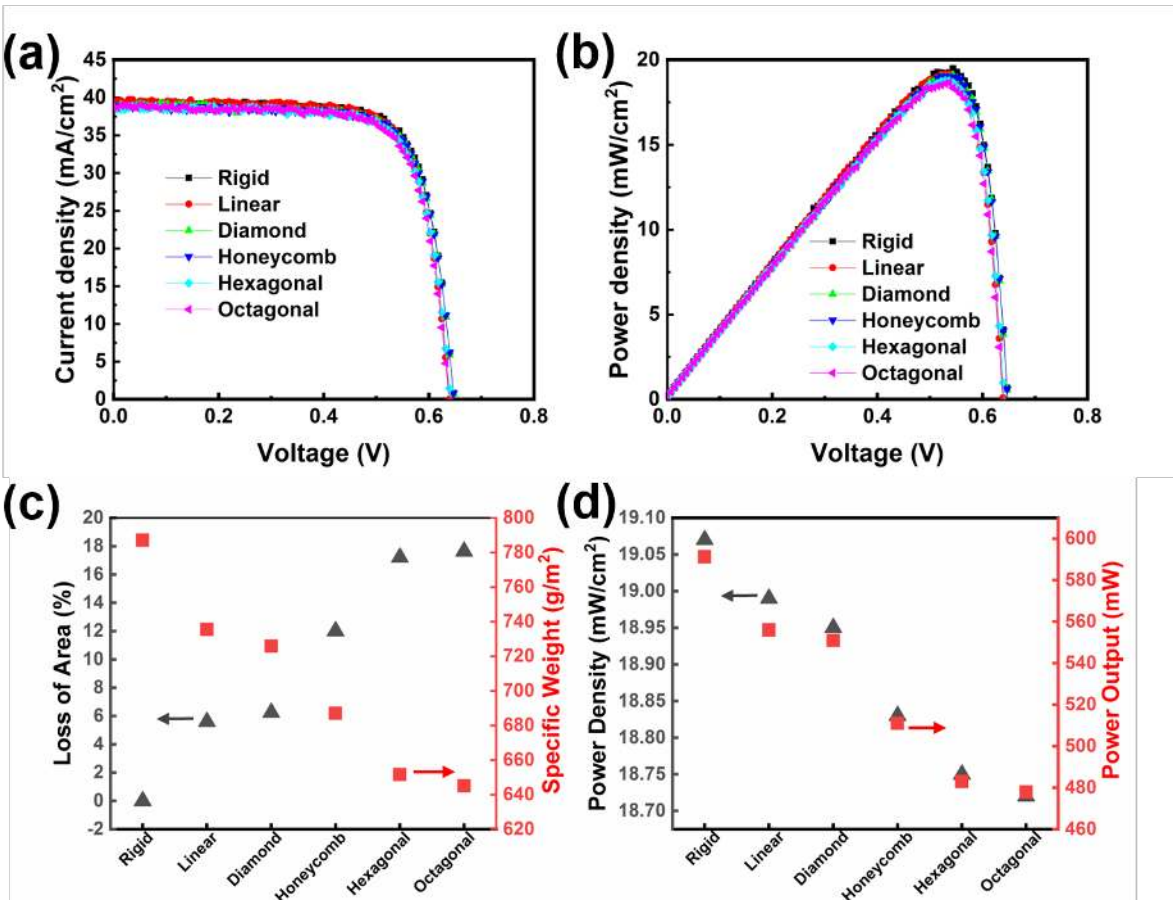

Figure 4. (a) Measured current density-voltage (J-V) characteristic of the rigid and corrugated photovoltaic cells. (b) Measured power density-voltage (P-V) performance of the rigid and corrugated cells. Area loss is taken into consideration in the calculation. (c) Measured loss of area in the corrugated cells in addition to the calculated corresponding specific weight. (d) Calculated power density and measured power output from the different corrugated solar cells. Actual area of the solar cell is used in the calculation (loss of area is not included).

2.3. Mechanical Resilience of the Flexible Solar Cells

To study the mechanical resilience of the flexible solar cells, the electrical performance is studied under different bending radii (Figure 5a). The projection area of the flexible cells is used to calculate the J_{sc} and Ƞ characteristics. Cycling tests, up to 500 cycles, are also conducted on

the flexible solar cells when bent with a 2 cm bending radius (Figure 5b) using a 3D printed apparatus (Figure 5c). The results show negligible degradation in the electrical performance when the corrugated solar cells are flexed down to 2 cm and up to 500 cycles, which confirms the robust performance of the developed flexible cells. In addition, a mechanical shock test is conducted on the encapsulated solar cells by dropping them from heights of 30 m using a drone and 15 m (Videos S1-S2). No cracks are observed in the flexible solar cells after the drop test, in addition, their efficiency is preserved which suggests that the PDMS absorbs the mechanical shock and protects the silicon cells. It is worth to mention that an unencapsulated rigid silicon solar cell would shatter when dropped from a height of 2 m.

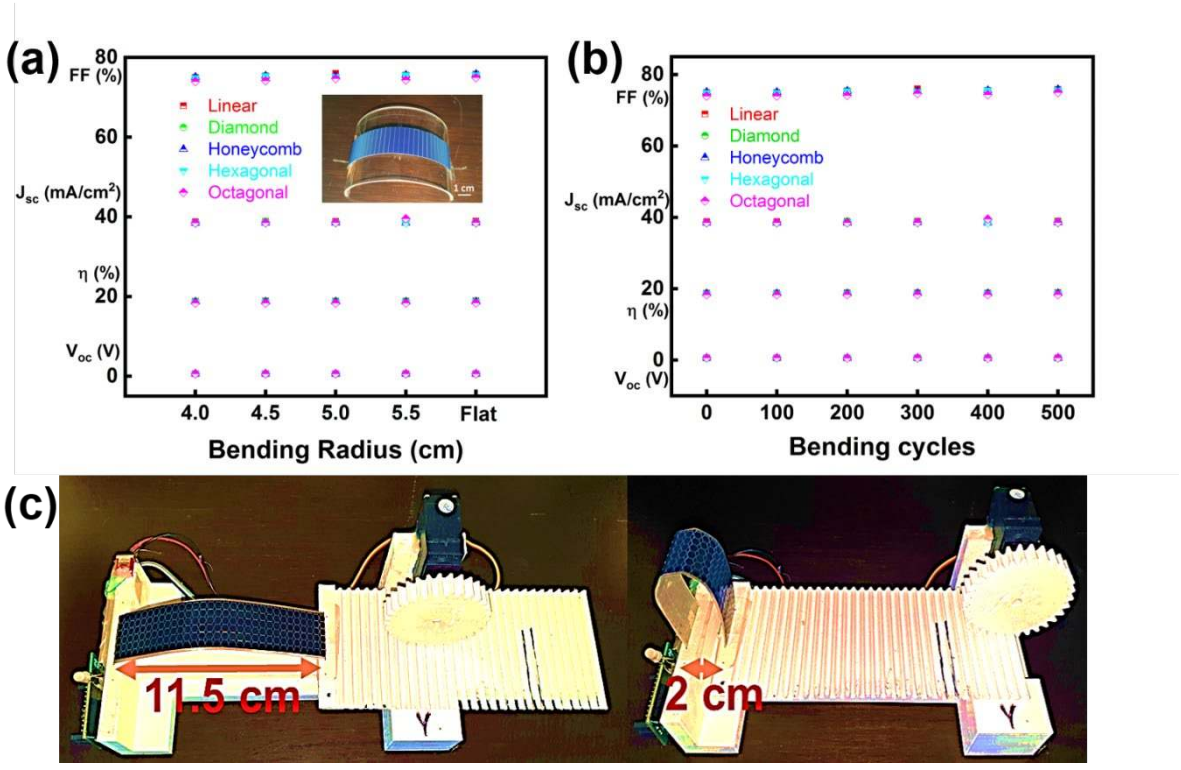

Figure 5. (a) Electrical performance of the corrugated solar cells when bent with a bending radius down to 4 cm. (b) Measured electrical performance of the corrugated

solar cells when bent with a 2 cm bending radius up to 500 cycles. (c) Optical image of the corrugated solar cells during the pre-bent and bent conditions.

2.4. Thermal Performance and Reliability of the Corrugated Solar Cells

The electrical performance of silicon solar cells is highly dependent on their actual temperature, in specific, monocrystalline silicon solar cells's efficiency drops by ~0.5% for every 1˚C rise in their temperature. The corrugation technique, by creating grooves within silicon, results in a fin-like architechture with an increased surface area-to-volume ratio which helps in improving the thermal dissipation by natural convection. In fact, the finned architecture has been widely used to improve the thermal dissipation characteristic of heat sinks.[35-36] To prove this, the temperature distribution on the rigid and linear corrugated solar cells is examined under an infrared microscope when both cells are exposed to light for 5 min with a 45˚ incident angle. The flexible linear patterned solar cell shows a reduction in temperature by 6.3% (Figure 6a, Video S3). while diamond patterned solar cell shows a 6.8% reduction in the temperature with respect to its rigid version (Figure S5). In this case, the solar cells are shone with light using an incadescent lamp, thus, heat in the cells is generated in two ways: heat due to the incadescent lamp and heat due to the phonons generated from the light-exposed silicon. The results depict that the linear corrugated solar cells show an improved thermal dissipation by natural convection as a result of the larger surface area-to-volume ratio, in addition to a reduced thermal conduction due to the air/PDMS gaps with high thermal resistivity in between the silicon islands. The latter property becomes important when the flexible solar cell is installed on a curved surface where the different areas on the cell receive sunlight with varied incident angles. The surfaces receving sunlight with a 0˚ incident angle have the highest absorption efficiency and therefore heat up the

most. In this case, the low thermal conduction in the corrugated structures would reduce the heat effect on the different areas of the flexible solar cell resulting in a higher overall efficiency.

Moreover, the thermal performance of the rigid and flexible solar cells is studied where both cells are exposed to 1 Sun AM 1.5G using a solar simulator for 16.5 continuous minutes. In this case the heat effect is mainly due to phonons generated from the light-exposed silicon. The efficiency of the solar cells is then monitored throughout the light exposure (Figure 6b). The results show that the higher the area loss due to the corrugation technique, the better the heat dissipation as a result of the larger surface area-to-volume ratio. In fact, the linear patterned solar cell provides a 7% increase in surface area-to-volume ratio and shows a reduction in temperature by 2.5%, while the octagonal patterned solar cell provides a 26% increase in surface area-to-volume ratio and shows a 14.6% reduction in temperature w.r.t the rigid solar cell. Thus, the results indicate that the corrugation technique improves the thermal dissipation in solar cells by natural convection.

Solar cells are generally encapsulated with a transparent material to protect them from environmental effects that accelerate their electrical degradation. However, when the encapsulated solar cells are exposed to sunlight, they generate heat which poses a new problem: thermal expansion mismatch between the solar cell and the encapsulation material. As a matter of fact, flexible solar cells are generally encapsulated with flexible polymeric materials which usually have a higher coefficient of thermal expansion (e.g. 3×10^{-4}/°C for PDMS) than silicon (2.6×10^{-6}/°C).[37] As a result, when heat is generated, the solar cell structure would bow upwards resulting in cracks within the silicon, degrading the solar cell's efficiency. Thus, the mitigation of the thermal expansion mismatch between the flexible solar cell and its encapsulant is a critical issue. The corrugation structure with grooves within the silicon allows the PDMS polymeric

material to fully encapsulate the silicon islands, thus allowing them to expand without bowing or cracking as depicted in Figures 6c-d where both encapsulated rigid and corrugated cells are heated up to 90˚C.

Finally, different environmental reliability tests are conducted on the flexible solar cells to study the robustness of PDMS as an encapsulation material. The environmental tests include immersion in multiple solutions such as water, sulfuric acid and ice to emulate different weather conditions such as rain, acidic rain and snow, respectively. The transmisson characteristic of the PDMS is studied before and after the environmental tests where an insignifican effect is observed (Figure 6e). In addition, the electrical performance of the encapsulated solar cells show negligible degradation in the performance which confirms the good encapsulation and isolation of the silicon solar cells from the outer effects (Figure 6f). It is worth to note that accelerated aging tests using concentrated UV tests on silicone based and EVA encapsulants have been studied extensively in the past where PDMS is found to be the most stable encapsulant.[38]

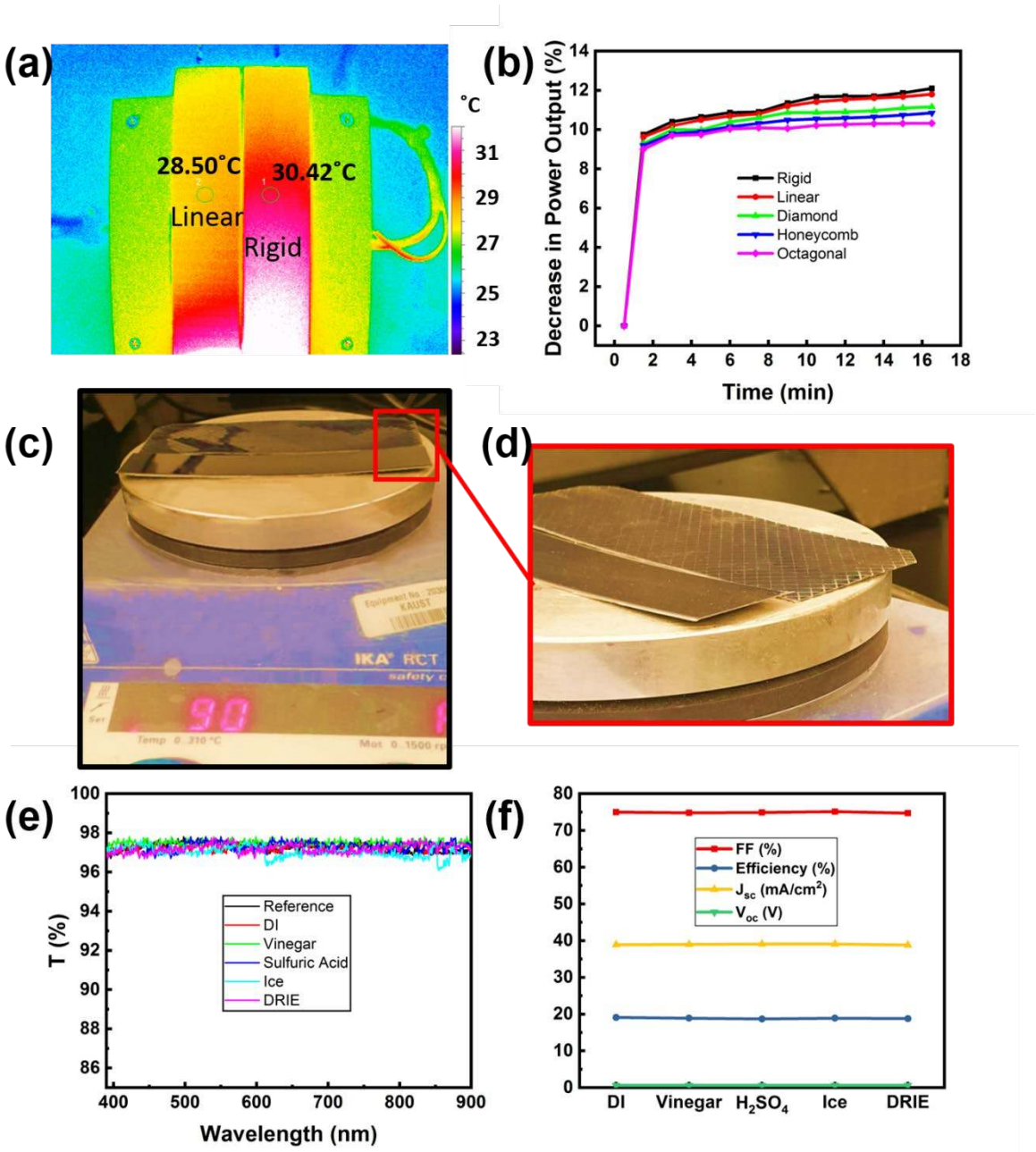

Figure 6. (a) Thermal image of the rigid and linear corrugated solar cells when exposed to light with 45˚ incident angle for 3 min. (b) Reduction in the power output of the different corrugated solar cells when exposed to 1-sun radiation up to 16 min. (c) Optical image of the rigid and diamond corrugated solar cells, encapsulated with PDMS and heated up to 90 ˚ C. (d) Inset from Figure 6c showing the bowing effect. (e)

Transmittance characteristic of the PDMS encapsulation layer when exposed to different environmental conditions. (f) Electrical performance of the PDMS encapsulated solar cell when exposed to different environmental conditions.

2. CONCLUSIONS

In conclusion, we have demonstrated a laser-patterning based corrugation process that allows the conversion of large-scale rigid photovoltaic cells based on the IBC technology into an ultra-flexible version with a preserved efficiency. Different corrugated patterns are shown to enable different capabilities in terms of ultra-flexibility, weight and output power. Thus, the presented results provide a guideline to follow in order to meet the requirements of specific applications of the flexible solar cells. The corrugation technique is shown to improve the thermal dissipation in the flexible solar cells by natural convection as a result of the larger surface area-to-volume ratio. Thus, solar cells with a larger active silicon area loss show a higher thermal dissipation rate. In addition, heat transfer by conduction between the different silicon islands is reduced due to the low thermal conductivity of the air/PDMS gaps in between the islands. The corrugated architecture also helps in relieving the thermal mismatch issue between the solar cell and its encapsulation material. A transparent and flexible polymeric material, PDMS, is used in this work to encapsulate and protect the flexible cells form the outer environment effect. The presented results confirm that the PDMS isolates well the silicon cells from different environmental effects such as rain and snow, in addition, it absorbs the mechanical shocks resulting in ultra-flexible solar cells with an excellent mechanical resilience.

3. MATERIALS AND METHODS

4.1. Fabrication of the Ultra-Flexible Cells

The flexible solar cells are fabricated by applying a corrugation process. This technique is based on a combination of CO_2 laser patterning and DRIE etching. The flexing process is performed on commercially available monocrystalline silicon solar cells based on the IBC technology with 19% efficiency. The Polydimethylsiloxane (PDMS) encapsulant is prepared by mixing the base silicone elastomer (Sylgard 184) with its curing agent using a 10:1 ratio. The PDMS is mixed in a vacuum mixer (THINKY Planetary Vacuum Mixer) with a 700 rpm speed and a 1.1 kPa pressure for 4 minutes to get rid of air bubbles. Then, 160 μm of PDMS is spin coated on a 25 in^2 commercial silicon solar cell and cured at 60˚C for 2 hours. A CO_2 laser (Universal Laser Systems PLS6.75) is then used to pattern PDMS with a speed of 40 mm/s, power of 24 W and a z-height of 1 mm. The exposed area is next etched using our pre-developed recipe using sulfur hexafluoride (SF_6) and carbon fluoride (C_4F_8) in a DRIE system at -20˚C and 30 mtorr.[31] The solar cells are again encapsulated in PDMS to protect the exposed areas. Area loss was measured using the KLONK software.[31] SEM images are obtained using a NOVA system with a 5 kV acceleration voltage and a 58 pA current.[31]

4.2. Characterizations and Measurements

The current density-voltage and power density-voltage characteristics are obtained using a Newport solar simulator linked to a Keithley source meter under 1 sun illumination at AM 1.5 G with intensity 1000 Wm^{-2} intensity.[31] The calibration is completed using a reference cell that is qualified by Newport. The J−V curves are measured from 1 V to −1.2 V along the reverse scan direction. The step voltage and scan speed are fixed at 7.35 mV and 82 $mV\,s^{-1}$,

respectively.[31] The original temperature of all solar cell structures was adjusted to 21˚C before performing the characterization under 1 sun illumination using the solar simulator. Transmittance data is measured using a UV-Vis spectrophotometer system (Thermo Evolution 600).

4.3. Environmental Testing

The encapsulated solar cells were immersed in water for 24 hours to emulate rain, in vinegar solution with a pH 2.2 for 96 hours, in sulfuric acid with pH 2 for 24 hours to emulate acidic rain and in ice to emulate a snowy weather. The solar cells were also stored in a DRIE chamber at -20˚C for 3 hours.

4.4. Thermal Measurements

The temperature distribution on the rigid and flexible solar cells was measured using an infrared microscope (OptoTherm). The original temperature of all solar cell structures was adjusted to 21˚C before performing the characterization under 1 sun illumination using the solar simulator or to light using an incandescent lamp.

4.5. Mechanical Shock Test

A drone (Phantom DJI) has been used to drop the solar cells from heights up to 30 m. A dropping system has been 3D printed and connected to the drone through a microcontroller.

ASSOCIATED CONTENT

The Supporting Information is available free of charge on the ACS Publications website. Supporting information includes additional data about loss of area calculation, heat dissipation tests and mechanical shock tests.

AUTHOR INFORMATION

Corresponding author email: muhammad.hussain@kaust.edu.sa and mmhussain@berkeley.edu, phone number: +966-544-700-072, group website: www.mmhlabs.org

Notes. The authors declare no competing financial interest.

ACKNOWLEDGMENT

M.M.H. conceived and directed the project. N.E.-A. led the fabrication, characterization, and analysis of the solar cells. R.A. aided in conducting the dropping test using the drone. R. Shamsuddin assisted in calculating the loss of area in the different solar cells. The findings were discussed by all the authors. The authors acknowledge support provided by the King Abdullah University of Science and Technology (KAUST) Office of Sponsored Research (OSR) under Award No. Sensor Innovation Initiative OSR-2015-Sensors-2707 and KAUST-KFUPM Special Initiative OSR-2016-KKI-2880.

REFERENCES

(1) Bauer, S.; Bauer-Gogonea, S.; Graz, I.; Kaltenbrunner, M.; Keplinger, C.; Schwödiauer, R. 25Th Anniversary Article: A Soft Future: From Robots And Sensor Skin To Energy Harvesters. *Advanced Materials* 2013, *26* (1), 149-162.

(2) Lee, J.; Xu, R.; Lee, S.; Jang, K.; Yang, Y.; Banks, A.; Yu, K.; Kim, J.; Xu, S.; Ma, S.; Jang, S.; Won, P.; Li, Y.; Kim, B.; Choe, J.; Huh, S.; Kwon, Y.; Huang, Y.; Paik, U.; Rogers, J. Soft, Thin Skin-Mounted Power Management Systems And Their Use In Wireless Thermography. *Proceedings of the National Academy of Sciences* 2016, *113* (22), 6131-6136.

(3) Hwang, G.; Yang, J.; Yang, S.; Lee, H.; Lee, M.; Park, D.; Han, J.; Lee, S.; Jeong, C.; Kim, J.; Park, K.; Lee, K. A Reconfigurable Rectified Flexible Energy Harvester Via Solid-State Single Crystal Grown PMN-PZT. *Advanced Energy Materials* 2015, *5* (10), 1500051-1500059.

(4) Lipomi, D.; Bao, Z. Stretchable, Elastic Materials And Devices For Solar Energy Conversion. *Energy & Environmental Science* 2011, 4 (9), 3314-3328.

(5) Kutbee, A.; Bahabry, R.; Alamoudi, K.; Ghoneim, M.; Cordero, M.; Almuslem, A.; Gumus, A.; Diallo, E.; Nassar, J.; Hussain, A.; Khashab, N.; Hussain, M. Flexible And Biocompatible High-Performance Solid-State Micro-Battery For Implantable Orthodontic System. *npj Flexible Electronics* 2017, *1* (1).

(6) Gao, Z.; Bumgardner, C.; Song, N.; Zhang, Y.; Li, J.; Li, X. Cotton-Textile-Enabled Flexible Self-Sustaining Power Packs Via Roll-To-Roll Fabrication. *Nature Communications* 2016, *7* (1).

(7) Wang, C.; Guan, L.; Zhao, D.; Yu, Y.; Grice, C.; Song, Z.; Awni, R.; Chen, J.; Wang, J.; Zhao, X.; Yan, Y. Water Vapor Treatment Of Low-Temperature Deposited Sno2 Electron Selective Layers For Efficient Flexible Perovskite Solar Cells. *ACS Energy Letters* 2017, *2* (9), 2118-2124.

(8) Albrecht, S.; Saliba, M.; Correa Baena, J.; Lang, F.; Kegelmann, L.; Mews, M.; Steier, L.; Abate, A.; Rappich, J.; Korte, L.; Schlatmann, R.; Nazeeruddin, M.; Hagfeldt, A.; Grätzel, M.; Rech, B. Monolithic Perovskite/Silicon-Heterojunction Tandem Solar Cells Processed At Low Temperature. *Energy & Environmental Science* 2016, *9* (1), 81-88.

(9) McMeekin, D.; Sadoughi, G.; Rehman, W.; Eperon, G.; Saliba, M.; Horantner, M.; Haghighirad, A.; Sakai, N.; Korte, L.; Rech, B.; Johnston, M.; Herz, L.; Snaith, H. A Mixed-Cation Lead Mixed-Halide Perovskite Absorber For Tandem Solar Cells. *Science* 2016, *351* (6269), 151-155.

(10) Park, N.; Grätzel, M.; Miyasaka, T.; Zhu, K.; Emery, K. Towards Stable And Commercially Available Perovskite Solar Cells. *Nature Energy* 2016, *1* (11).

(11) Li, Y.; Xu, G.; Cui, C.; Li, Y. Flexible and Semitransparent Organic Solar Cells. *Advanced Energy Materials* 2017, *8* (7), 1701791-1701829.

(12) Voggu, V.; Sham, J.; Pfeffer, S.; Pate, J.; Fillip, L.; Harvey, T.; Brown, R.; Korgel, B. Flexible $CuInSe_2$ Nanocrystal Solar Cells On Paper. *ACS Energy Letters* 2017, *2* (3), 574-581.

(13) Cong, S.; Zou, G.; Lou, Y.; Yang, H.; Su, Y.; Zhao, J.; Zhang, C.; Ma, P.; Lu, Z.; Fan, H.; Huang, Z. Fabrication Of Nickel Oxide Nanopillar Arrays On Flexible Electrodes For Highly Efficient Perovskite Solar Cells. *Nano Letters* 2019, *19* (6), 3676-3683.

(14) Battaglia, C.; Cuevas, A.; De Wolf, S. High-Efficiency Crystalline Silicon Solar Cells: Status And Perspectives. *Energy & Environmental Science* 2016, *9* (5), 1552-1576.

(15) Fields, J.; Ahmad, M.; Pool, V.; Yu, J.; Van Campen, D.; Parilla, P.; Toney, M.; van Hest, M. The Formation Mechanism For Printed Silver-Contacts For Silicon Solar Cells. *Nature Communications* 2016, *7* (1).

(16) Bullock, J.; Hettick, M.; Geissbühler, J.; Ong, A.; Allen, T.; Sutter-Fella, C.; Chen, T.; Ota, H.; Schaler, E.; De Wolf, S.; Ballif, C.; Cuevas, A.; Javey, A. Efficient Silicon Solar Cells With Dopant-Free Asymmetric Heterocontacts. *Nature Energy* 2016, *1* (3).

(17) Cuevas, A.; Sinton, R.; Midkiff, N.; Swanson, R. 26-Percent Efficient Point-Junction Concentrator Solar Cells With A Front Metal Grid. *IEEE Electron Device Letters* 1990, *11* (1), 6-8.

(18) Kerschaver, E.; Beaucarne, G. Back-Contact Solar Cells: A Review. *Progress in Photovoltaics: Research and Applications* 2006, *14* (2), 107-123.

(19) Bullock, J.; Wan, Y.; Xu, Z.; Essig, S.; Hettick, M.; Wang, H.; Ji, W.; Boccard, M.; Cuevas, A.; Ballif, C.; Javey, A. Stable Dopant-Free Asymmetric Heterocontact Silicon Solar Cells With Efficiencies Above 20%. *ACS Energy Letters* 2018, *3* (3), 508-513.

(20) Yoshikawa, K.; Kawasaki, H.; Yoshida, W.; Irie, T.; Konishi, K.; Nakano, K.; Uto, T.; Adachi, D.; Kanematsu, M.; Uzu, H.; Yamamoto, K. Silicon Heterojunction Solar Cell With Interdigitated Back Contacts For A Photoconversion Efficiency Over 26%. *Nature Energy* 2017, *2* (5).

(21) Masuko, K.; Shigematsu, M.; Hashiguchi, T.; Fujishima, D.; Kai, M.; Yoshimura, N.; Yamaguchi, T.; Ichihashi, Y.; Mishima, T.; Matsubara, N.; Yamanishi, T.; Takahama, T.; Taguchi, M.; Maruyama, E.; Okamoto, S. Achievement Of More Than 25% Conversion Efficiency With Crystalline Silicon Heterojunction Solar Cell. *IEEE Journal of Photovoltaics* 2014, *4* (6), 1433-1435.

(22) Lu, M.; Bowden, S.; Das, U.; Birkmire, R. Interdigitated Back Contact Silicon Heterojunction Solar Cell And The Effect Of Front Surface Passivation. *Applied Physics Letters* 2007, *91* (6), 063507-063510.

(23) Franklin, E.; Fong, K.; McIntosh, K.; Fell, A.; Blakers, A.; Kho, T.; Walter, D.; Wang, D.; Zin, N.; Stocks, M.; Wang, E.; Grant, N.; Wan, Y.; Yang, Y.; Zhang, X.; Feng, Z.; Verlinden, P. Design, Fabrication And Characterisation Of A 24.4% Efficient Interdigitated Back Contact Solar Cell. *Progress in Photovoltaics: Research and Applications* 2014, *24* (4), 411-427.

(24) Yoshikawa, K.; Yoshida, W.; Irie, T.; Kawasaki, H.; Konishi, K.; Ishibashi, H.; Asatani, T.; Adachi, D.; Kanematsu, M.; Uzu, H.; Yamamoto, K. Exceeding Conversion Efficiency Of 26% By Heterojunction Interdigitated Back Contact Solar Cell With Thin Film Si Technology. *Solar Energy Materials and Solar Cells* 2017, *173*, 37-42.

(25) Rahman, T.; To, A.; Pollard, M.; Grant, N.; Colwell, J.; Payne, D.; Murphy, J.; Bagnall, D.; Hoex, B.; Boden, S. Minimising Bulk Lifetime Degradation During The Processing Of Interdigitated Back Contact Silicon Solar Cells. *Progress in Photovoltaics: Research and Applications*2017, *26* (1), 38-47.

(26) Savin, H.; Repo, P.; von Gastrow, G.; Ortega, P.; Calle, E.; Garín, M.; Alcubilla, R. Black Silicon Solar Cells With Interdigitated Back-Contacts Achieve 22.1% Efficiency. *Nature Nanotechnology* 2015, *10* (7), 624-628.

(27) Yoon, J.; Li, L.; Semichaevsky, A.; Ryu, J.; Johnson, H.; Nuzzo, R.; Rogers, J. Flexible Concentrator Photovoltaics Based On Microscale Silicon Solar Cells Embedded In Luminescent Waveguides. *Nature Communications* 2011, *2* (1).

(28) Branham, M.; Hsu, W.; Yerci, S.; Loomis, J.; Boriskina, S.; Hoard, B.; Han, S.; Chen, G. 15.7% Efficient 10-Mm-Thick Crystalline Silicon Solar Cells Using Periodic Nanostructures. *Advanced Materials* 2015, *27* (13), 2182-2188.

(29) Rahman, A.; Ashraf, A.; Xin, H.; Tong, X.; Sutter, P.; Eisaman, M.; Black, C. Sub-50-Nm Self-Assembled Nanotextures For Enhanced Broadband Antireflection In Silicon Solar Cells. *Nature Communications* 2015, *6* (1).

(30) Bahabry, R.; Kutbee, A.; Khan, S.; Sepulveda, A.; Wicaksono, I.; Nour, M.; Wehbe, N.; Almislem, A.; Ghoneim, M.; Torres Sevilla, G.; Syed, A.; Shaikh, S.; Hussain, M. Corrugation Architecture Enabled Ultraflexible Wafer-Scale High-Efficiency Monocrystalline Silicon Solar Cell. *Advanced Energy Materials* 2018, *8*, 1702221-1702230.

(31) El-Atab, Nazek; Qaiser, Nadeem; Bahabry, Rabab and Hussain, Muhammad Mustafa. Corrugation Enabled Asymmetrically Ultra-Stretchable (95%) Monocrystalline Silicon Solar Cells with High Efficiency (19%). *Adv. Energy Mater.* 2019, 1902883-1902890. DOI: 10.1002/aenm.201902883

(32) Lee, K.; Hwang, I.; Kim, N.; Choi, D.; Um, H.; Kim, S.; Seo, K. 17.6%-Efficient Radial Junction Solar Cells Using Silicon Nano/Micro Hybrid Structures. *Nanoscale* 2016, *8* (30), 14473-14479.

(33) Zhang, Y.; Liu, H. Nanowires For High-Efficiency, Low-Cost Solar Photovoltaics. *Crystals* 2019, *9*, 87-112.

(34) Shaeri, M.; Bonner, R. Analytical Heat Transfer Model For Laterally Perforated-Finned Heat Sinks. *International Journal of Heat and Mass Transfer* 2019, *131*, 1164-1173.

(35) Wei, X.; Zhang, T.; Luo, T. Molecular Fin Effect From Heterogeneous Self-Assembled Monolayer Enhances Thermal Conductance Across Hard–Soft Interfaces. *ACS Applied Materials & Interfaces* 2017, *9* (39), 33740-33748.

(36) Wei, X.; Zhang, T.; Luo, T. Thermal Energy Transport Across Hard–Soft Interfaces. *ACS Energy Letters* 2017, *2* (10), 2283-2292.

(37) Kim, B.; Park, M.; Kim, Y.; Jeong, U. Thermal Expansion and Contraction Of An Elastomer Stamp Causes Position-Dependent Polymer Patterns In Capillary Force Lithography. *ACS Applied Materials & Interfaces* 2011, *3* (12), 4695-4702.

(38) McIntosh, K.; Powell, N.; Norris, A.; Cotsell, J.; Ketola, B. The Effect of Damp-Heat And UV Aging Tests On The Optical Properties Of Silicone And EVA Encapsulants. *Progress in Photovoltaics: Research and Applications* 2010, *19* (3), 294-300.

TOC GRAPHICS